LA-UR -81-1882

Los Alamos National Laboratory is operated by the University of California for the United States Department of Energy under contract W-7405-ENG-36

MASTER

TITLE COMPUTATION OF HIGH REYNOLDS NUMBER INTERNAL/EXTERNAL FLOWS

AUTHOR(S) M. C. Cline and R. G. Wilmoth

SUBMITTED TO AIAA 14th Fluid and Plasma Dynamics Conference, Palo Alto, CA, June 23-25, 1981

Los Alamos Los Alamos National Laboratory
Los Alamos, New Mexico 87545

COMPUTATION OF HIGH REYNOLDS NUMBER INTERNAL/EXTERNAL FLOWS

by

Michael G. Cline
Los Alamos National Laboratory
Los Alamos, NM 87545

and

Richard G. Wilmoth
NASA Langley Research Center
Hampton, VA 23665

Abstract

A general, user oriented computer program, called VNAP2, has been developed to calculate high Reynolds number, internal/external flows. VNAP2 solves the two-dimensional, time-dependent Navier-Stokes equations. The turbulence is modeled with either a mixing-length, a one transport equation, or a two transport equation model. Interior grid points are computed using the explicit MacCormack scheme with special procedures to speed up the calculation in the fine grid. All boundary conditions are calculated using a reference plane characteristic scheme with the viscous terms treated as source terms. Several internal, external, and internal/external flow calculations are presented.

Introduction

The computation of high Reynolds number flows has become a major tool in the analysis and design of aerospace vehicles. While Navier-Stokes solutions for complete vehicle configurations are still beyond the limits of present-day computers, computational techniques are used routinely in the analysis and design of various individual components, e.g., airfoils, wing-body combinations, inlets and nozzles. Most of these analyses use either purely inviscid or the so-called matched viscous-inviscid techniques due to their greater computational efficiency and ease of use over the more exact Navier-Stokes solution methods. These approximate techniques often yield results of surprisingly high accuracy.[1] However, their use is generally limited to problems involving weak viscous-inviscid interactions or to strong interactions that are sufficiently well understood to be modeled empirically.

Navier-Stokes (N-S) solution methods, on the other hand, are not subject to these fundamental limitations and are applicable to more general classes of flow problems. However, the N-S methods have not found widespread use for design purposes due primarily to their expense and difficulty of use. Computer run times of several hours are not uncommon in solving a high Reynolds number problem in which the viscous layer must be well resolved. Furthermore, application of N-S methods is often viewed by the engineer as an art requiring extensive knowledge of the numerical algorithm and considerable trial and error to obtain a correct, converged solution. The latter is often the result of attempting to use a N-S computer code which has been written to solve a very specific class of problems and may not be sufficiently general, well-documented, and user-oriented. Clearly, as more efficient N-S algorithms and larger, faster computers become available, more attention must be given to the development of user-oriented N-S codes if they are to receive practical application.

The purpose of this paper is to describe a N-S computer program, VNAP2,[2] which has evolved over a period of several years for solving a relatively wide class of steady and unsteady, internal and external flow problems. VNAP2 is a modified version of VNAP[1] and solves the two-dimensional (axisymmetric), time-dependent, compressible Navier-Stokes equations. Both single and dual flowing streams may be solved. The flow boundaries may be arbitrary curved solid walls, inflow/outflow boundaries, or free-jet envelopes. Turbulent as well as laminar and inviscid flows may be treated. Some typical internal and external flow geometries that may be solved are shown in Fig. 1. Although the VNAP2 code has been applied mainly to nozzle and inlet flows, the relatively general treatment of geometries and flow boundaries allows a variety of other problems to be solved, e.g., airfoils, flow-through nacelles, free-shear flows and free-jet expansions.

In this paper, the methodology used in developing VNAP2 as a user-oriented, production-type computer program is presented and some results obtained in solving a variety of flow problems are shown. Although the results, in some cases, point out the need for further improvements in both numerical and physical modeling, they do illustrate, to a great extent, that practical Navier-Stokes applications are possible.

Governing Equations

The VNAP2 code solves the two dimensional (axisymmetric), time dependent, Navier-Stokes equations. The turbulence is modeled using either a mixing-length, a one transport equation or a two transport equation model. The mixing length model employs the Launder et al.[6] model for free shear layers and the Cebeci-Smith[7] model for boundary layers. The one equation model is that of Daly[8] while the two equation model is the Jones-Launder[9,10] model. For details of these turbulence models, including boundary conditions, see Ref. 2. VNAP2 employs an explicit artificial viscosity to stabilize the calculations for shock waves. This artificial viscosity is used in place of the fourth-order smoothing usually employed by MacCormack.[11] For details of the governing equations see Ref. 2.

[a] Group P-1, Member AIAA

[b] Propulsion Aerodynamics Branch

Physical and Computational Flow Spaces.

The physical flow space geometry is shown in Fig. 2. The flow is from left to right. The upper boundary, called the wall, can be either a solid boundary, a free jet boundary, or an arbitrary subsonic (normal to the boundary) inflow/outflow boundary. The lower boundary, called the centerbody, can be either a solid boundary or a plane (line) of symmetry. The geometry can be either a single flowing stream or, if the dual flow space walls are present, a dual flowing stream. The dual flow space walls, shown in Fig. 2, may begin in the interior and continue to the exit (inlet geometry), may begin at the inlet and terminate in the interior (afterbody geometry), as shown in Fig. 2, or may begin and end in the interior (airfoil geometry). All of the above boundaries may be arbitrary curved boundaries provided the y coordinate is a single value function of x. This single value function of x requires dual flow space walls, that begin or terminate in the interior, do so with pointed ends. The points can be very blunt, but cannot be vertical walls. The left boundary is a subsonic, supersonic, or mixed inflow boundary while the right boundary is a subsonic, supersonic, or mixed outflow boundary or a subsonic inflow boundary.

The physical space grid has the following properties: one set of grid lines are straight and in the y direction with arbitrary spacing in the x direction; the second set of grid lines approximately follow the wall and centerbody contours; the Δy spacing of these grid lines is arbitrary at one x location and is proportional to those values at any other x location.

The x, y physical space is mapped into a rectangular ξ, η computational space as shown in Fig. 2. The mapping is carried out in two parts - the first part maps the physical space to a rectangular computational space while the second maps the variable grid computational space to a uniform grid computational space. Both the upper and lower dual flow space walls collapse to the the same grid line in the computational space, as shown in Fig. 2. The flow variables at the grid points on the upper dual flow space wall are stored in the regular solution array while the variables at the lower dual flow space wall are stored in a dummy array. These flow variables are continually switched between these two arrays during the calculation. For details of the transformations, see Ref. 2.

Numerical Method

The computational plane grid points are divided up into interior and boundary points. The boundary grid points are further divided up into left boundary, right boundary, wall, centerbody, and dual flow space wall points (see Fig. 2).

Interior Grid Points

The interior grid points are computed using the unsplit MacCormack scheme.[12] The governing equations are left in nonconservation form. In order to improve the computational efficiency for high Reynolds number flows, the grid points in fine part of the grid may be subcycled. This is accomplished by first computing the grid points in the coarse part of the grid for one time step Δt. Next, the grid points in the fine grid are calculated k times, where k is an integer, with a time step $\Delta t/k$. The grid points at the edge of the fine grid require a special procedure, because one of their neighboring points is calculated as part of the coarse grid. Except for the first subcycled time step, this point is unknown. However, the values at t and $t+\Delta t$ are known from the coarse grid solution and, so, the values between t and $t+\Delta t$ are determined by linear interpolation.

In order to further improve the computational efficiency, a special procedure is employed to increase the allowable time step in the subcycled part of the grid. This procedure allows the removal of the sound speed from the time step C-F-L condition. Procedures that accomplished this have been proposed by Harlow and Amsden[13] and MacCormack.[14] The procedure of Harlow and Amsden is an implicit scheme that removes the sound speed, in both the x and y directions, by an implicit treatment of the mass equation and the pressure gradient terms in the momentum equations. MacCormack's procedure is explicit and removes the sound speed in only one direction. (MacCormack's procedure also includes an implicit procedure to remove the viscous diffusion restriction from the time step C-F-L condition.) Because explicit schemes are easier to program for efficient computation on vector computers and because high Reynolds number flows usually required fine grid spacing in only one direction, it was decided to use a procedure similar to that of MacCormack.

MacCormack's procedure is based on the assumption that the velocity component, in the coordinate direction with the fine grid spacing, is negligible compared to the sound speed. This allows the governing equations to be simplified. MacCormack then applies the Method of Characteristics to these simplified equations. However, for flows over bodies with large amounts of curvature as well as many free shear flows this assumption is questionable. Because VNAP2 is intended to be a general code for solving a wide variety of problems, this assumption was felt to be too restrictive. Therefore, the main difference between MacCormack's scheme and the one presented below is the removal of this restriction. This procedure, however, does assume that the flow in the y direction is subsonic.

The procedure here is to separate the governing equations into two parts. The first part consists of the Mach line characteristic compatibility equations while the streamline compatibility equations and all viscous terms make up the second part. Because the sound speed limitation is due to the first part, the second part can be computed by the standard MacCormack scheme. The first part of the governing equations is solved by a special procedure. This special procedure consists of selecting an increased time step based on $\Delta y/|v|$ instead of $\Delta y/(|v|+a)$ where v is the velocity component in the y direction and a is the sound speed. The Mach line characteristics are then extended back from the solution point at the increased time step. These characteristics will intersect the previous solution plane outside the computation star of the MacCormack scheme. By calculating these characteristic intersecting points, special differences using this increased domain of dependence can be determined and used in the first part of the governing equations. These special differences use a larger Δy than the MacCormack scheme and, therefore, are less accurate. However, this procedure is only used in boundary or free shear layers where the viscous terms dominate the solution. This special procedure decreases the

computational time for high Reynolds number flows by factors of 5 to 10 over flows that are not subcycled. For details of this procedure, see Ref. 2.

Left Boundary Grid Points

The left boundary can only be an inflow boundary. For supersonic inflow all flow variables are specified. For subsonic inflow, there are two different boundary condition options. The first specifies the total pressure p_T, total temperature T_T, and flow angle θ as proposed by Serra.[15] The second condition specifies the x and y velocity components u and v, respectively, along with the density ρ and was shown to be correct for a well-posed problem by Oliger and Sundström.[16] For a discussion of the relative merits of these two boundary conditions, see Ref. 2. Following the ideas of Moretti and Abbett,[17] all the unspecified dependent variables are computed using a reference plane characteristic scheme. The viscous terms are treated as source terms. For mixed subsonic-supersonic inflow, VNAP2 checks the Mach number at each grid point to determine the correct boundary condition. The u, v, and ρ boundary condition includes a nonreflecting option to eliminate the trapping of waves in subsonic, steady flows (see Ref. 2 for details).

Right Boundary Grid Points

The right boundary can be a supersonic outflow boundary or a subsonic inflow/outflow boundary. The subsonic inflow option is required for cases with flow separation at the right boundary. For supersonic outflow, all the variables are extrapolated. For subsonic outflow, the static pressure p is specified and the remaining variables are calculated using a reference plane characteristic scheme. If subsonic reverse flow occurs at the right boundary, inflow boundary conditions must be specified. This is accomplished by leaving p equal to the specified exit pressure and specifying ρ and v. This inflow boundary condition is also discussed by Oliger and Sundström.[16] These boundary conditions include the nonreflecting procedure of Rudy and Strikwerda.[18] For mixed subsonic-supersonic outflow, VNAP2 checks the Mach number to determine the correct boundary condition.

Wall Grid Points

The wall boundary can be a free-slip boundary, a free-jet boundary, a no-slip boundary, or a arbitrary inflow/outflow boundary. For the free-slip option, the wall slope is the boundary condition and the remaining variables are calculated using a reference plane characteristic scheme. For the free-jet boundary option, the static pressure is specified and the code determines the free-jet boundary. For the no-slip boundary, the velocity components are set to zero while either the temperature is specified or the temperature gradient is set to zero (adiabatic wall). The density is calculated by the reference plane characteristic scheme. For the arbitrary inflow/outflow boundary, the static pressure is specified. If the flow across the boundary is outfl the remaining variable are determined by the reference plane characteristic scheme. If inflow occurs, the velocity component tangent to the boundary and the density are specified while the normal velocity component is determined using the reference plane characteristic scheme. A nonreflecting boundary condition option is included.

Centerbody Grid Points

The centerbody boundary can be a free-slip boundary, a no-slip boundary, or a plane (axis) of symmetry. The free-slip and no-slip boundary calculations follow the wall procedure. For flows where the centerbody is a plane of symmetry, the grid points are computed by the interior point scheme. The boundary condition is the requirement of flow symmetry.

Dual Flow Space Wall Grid Points

The dual flow space walls can be either a free-slip or no-slip boundary. The calculations follow the wall and centerbody procedures.

Steady State Acceleration for Subsonic Flow

Because signals propagate in all directions in subsonic flows, disturbances can reflect around inside the computational grid for many time steps. This reflection of disturbances can significantly prolong the convergence to steady state. Several different procedures for accelerating the convergence to steady state for both the p_T, T_T, θ and u, v, ρ inflow boundary conditions are presented in Ref. 2. One technique that works well for very complex flows is an extended interval time smoothing procedure. Here, the solution for all dependent variables on the first time step is stored. The pressure at a specified grid point is then monitored on each time step. When this pressure changes direction, the solution at the current time step is averaged with the solution at the first time step. This averaged solution replaces the current time step solution and, in addition, is stored in place of the first time step solution. This averaging procedure is continued until the flow is steady. The results for subsonic, steady flow in a converging duct are shown in Fig. 3. The top curve is for a calculation in which the initial-data surface consisted of stationary flow at the stagnation pressure and temperature. At time equal to zero, the outflow pressure was dropped from the stagnation value to the desired value, thus simulating a bursting diaphragm. The middle curve is for a calculation in which the initial-data surface was the 1-D solution generated by the VNAP2 code. The bottom curve shows the calculation employing the 1-D initial-data surface and the extended interval time smoothing. All three solutions employed the p_T, T_T, and θ inflow boundary condition. From Fig. 3, we see that both improving the accuracy of the initial-data surface and employing the extended interval time smoothing significantly improved the convergence to a steady state. As a result, both procedures are utilized in the following results.

Results

The results presented here are for six high Reynolds number flows; one internal, two external and three internal/external cases. One case in each category has flow separation and the last case includes transition from laminar to turbulent flow. These cases represent very complex flows and as such were selected to illustrate the more difficult problems that VNAP2 is capable of solving. There is a considerable number of less complex viscous as well

as inviscid flows than VNAP2 can solve more accurately and with significantly less amounts of computer time. All cases were run with the unmodified VNAP2 code utilizing only a small data file. At this time, very few parametric studies to determine the optimum turbulence model parameters, initial-data surface quantities and grid point distributions, have been carried out. As a result, the accuracy and efficiency of these results do not necessarily represent the optimal use of the VNAP2 code.

Internal Flow

The internal flow case is nozzle B-3 of Ref. and is the planar, converging-diverging nozzle shown in Fig. 4. The flow is from left to right with the physical space grid enclosed by the dashed line. The Reynolds number based on the throat height is 7.7×10^5. At the left boundary, p_T is set equal to 200.6 kPa (29.1 psia), T_T is set equal to 300 K and θ is set equal to 0. At the right boundary, extrapolation is used when the flow is supersonic. When the flow is subsonic outflow, p is set equal to 101.4 kPa (14.7 psia). For subsonic inflow, in addition to specifying p, v is set equal to 0 and ρ is set equal to the average of the wall and midplane values. The wall is a no-slip boundary and the results presented here employed the two equation turbulence model. The initial conditions consisted of 1-D, inviscid flow that was sonic at the throat and subsonic downstream.

The physical space grid, Mach number and turbulence energy contours are shown in Fig. 5. The experimental data are from Ref. 19. From Fig. 5, we see that at this pressure ratio, the flow separates creating a reverse flow region. The wall and midplane pressures are shown in Fig. 6. This calculation used a 45 by 21 grid and required 3000 time steps (30,000 subcycled time steps) and 2.1 hours cpu time (CDC-7600) to reach steady state.

External Flow

The external flow cases are configs. 1 and 3 Ref. 20 and are the axisymmetric, boattail afterbody flows, with solid bodies simulating the exhaust jets shown in Fig. 7. The flow is from left to right with the physical space grid enclosed by the dashed line. The Reynolds number based on x at the left boundary is 1.05×10^7. The first case (ℓ = 27.0 cm) is config. 3 while the second (ℓ = 12.2 cm) is config. 1. Both cases consisted of the same flow conditions. The left boundary inflow profiles of ρ and T_T for a free stream Mach number of 0.8 were determined using the same inviscid/boundary layer procedure employed by Ref. 21. The flow angle θ was set equal to 0. At the right boundary p was set equal to the free stream value. The wall is an arbitrary inflow/outflow boundary. For outflow, p is set equal to the free stream value. When inflow occurs, in addition to specifying p, u and ρ are set equal to their free stream values. The centerbody is a no-slip boundary. Both calculations employed the extended interval time smoothing. The initial conditions consisted of extending the inflow profiles downstream to the right boundary.

The physical space grid, pressure and Mach number contours for config. 3 (ℓ = 27.0 cm), employing the mixing-length turbulence model, are shown in Fig. 8 while the surface pressure is shown in Fig. 9. The physical space grid, Mach number and turbulence energy contours for config. 1 (ℓ = 12.2 cm), employing the two equation turbulence model, are shown in Fig. 10 while the surface pressure is shown in Fig. 11. The experimental data, for both cases, are from Ref. 20. From these figures, we see that the flow for config. 3 remained attached while separation occured for config. 1. The mixing-length model produced slightly better results for config. 3. However, the two equation model more accurately predicted the pressure plateau in config. 1, but underpredicted the amount of upstream expansion. Swanson[21] found that a relaxation or lag model improved the pressure plateau prediction of the mixing-length model, but at the expense of also underpredicting the amount of upstream expansion. The config. 3 calculation, employing the mixing-length model, used a 40 by 25 grid and required 750 time steps (15,000 subcycled time steps) and 1.0 hours of CPU time (CDC-7600) to reach steady state. The config. 1 calculation, employing the mixing-length model, used a 47 by 29 grid and required 750 time steps (17,000 subcycled time steps) and 2.1 hours of CPU time (CDC-7600) to reach steady state. The two equation model computational times were 1.4 hours for config. 3 and 3.7 hours for config. 1.

Internal/External Flow

The first two cases are the two external flow cases presented above, but with the solid simulators replaced by the exhaust jets. The geometry is shown in Fig. 12 with the physical space grid enclosed by the dashed lines. The left external boundary, wall and right boundary are the same as the external cases. At the left internal boundary, p_T is set equal to 132.4 kPa (19.2 psia), T_T is set equal to 300 K and θ is set equal to 0. The free stream pressure is 65.2 kPa (9.45 psia). The centerbody is the flow centerline, while the dual flow space walls are no-slip boundaries. Again, both calculations employed the extended interval time smoothing. Only the two equation turbulence model was employed for these two cases. The initial conditions for these cases consisted of the external flow solutions presented above along with the 1-D, inviscid flow solution for the nozzle.

The physical space grid and Mach number contours for config. 3 (ℓ = 27.0 cm) are shown in Fig. 13. The external surface pressure is shown in Fig. 14 while the total pressure profiles for the shear layer, produced by the interaction between the exhaust jet and the external flow, are shown in Fig. 15. The physical space grid and Mach number contours for config. 1 (ℓ = 12.2 cm) are shown in Fig. 16. The external surface pressure is shown in Fig. 17 while the total pressure profiles for the shear layer are shown in Fig. 18. The experimental data, for both cases, are from Refs. 20 and 22. From Figs. 14 and 17, we see that the computed solutions, for both cases, underpredicted the shear layer spreading rate. The same trends were found in results generated by a patched method.[23] The config. 3

The last case is the NACA 1-89-100 inlet of Ref. 24 and is shown in Fig. 19. The flow is from left to right with the physical space grid enclosed by the dashed line. The Reynolds number based on the maximum external diameter is 6.1×10^6. At the left boundary, p_T was set equal to 101.4 kPa (14.7 psia), T_T was set equal to 294.4 K and θ was set equal to 0. The free stream pressure is 66.5 kPa (9.64 psia) which produces a free stream Mach number of 0.8. The wall is the arbitrary inflow/outflow boundary and uses the same boundary conditions as the previous two cases. At the right external boundary, the pressure was set equal to the measured values. In the experiments of Ref. 24, the internal flow rate was controlled by a throttling mechanism well downstream of the right boundary. In order not to compute this rather extensive flow region, a value of pressure was specified at the right internal boundary such that the inviscid, 1-D mass flow equalled the experimental value. The centerbody is the flow centerline, while the dual flow space walls are no-slip boundaries. The extended interval time smoothing was employed. The initial conditions consisted of 1-D, inviscid flow.

The physical space grid, Mach number and turbulence energy contours are shown in Fig. 20, while the surface pressure is shown in Fig. 21. The experimental data are from Ref. 24. From the turbulence energy contours in Fig. 20, we see that the flow over the inlet is initially laminar, but quickly becomes turbulent. The flow transitions first on the interior surface. Reference 24 did not give the transition locations. The surface pressures in Fig. 21, are for the first 6% of the inlet. This small area of interest, combined with the thin laminar boundary layer, required a very fine grid spacing in both coordinate directions. Because of the fine grid spacing in the x direction, the subcyling option was not used. The differences in surface pressure, between theory and experiment, at the inlet tip are probably the result of too coarse a grid. The difference, between theory and experiment, near the internal, right boundary is most likely due to the approximate treatment of the internal flow at this boundary. This calculation was also made using the mixing-length turbulence model, however, this model significantly overpredicts the level of turbulence upstream of the inlet. This is because the downstream blockage due to the presence of the inlet creates a weak shear layer profile upstream of the inlet that extends a large distance in the cross stream direction. Therefore, the mixing length model predicts very large mixing lengths. This produces turbulent viscosities, upstream of the inlet, that are several orders of magnitude larger than the molecular value. As a result, the mixing-length model solution is not presented here. This calculation used a 53 by 44 grid and required 3000 time steps and 1.0 hours of CPU time (CDC-7600) to reach steady state.

Conclusions

A general, user oriented computer program for computing high Reynolds number flows has been presented. Six high Reynolds number flow calculations were described. These computed results show that practical Navier-Stokes applications are possible. However, these results also indicate the need for better turbulence modeling for separated flows and more efficient solution algorithms for very nonuniform grid point distributions.

Acknowledgment

This work was supported by the Propulsion Aerodynamics Branch of the NASA Langley Research Center (LRC) and the U.S. Department of Energy. The authors would like to thank R. C. Swanson and L. E. Putnam of the LRC and B. J. Daly of the Los Alamos National Laboratory for many helpful discussions.

References

1. "Computation of Viscous-Inviscid Interaction," AGARD Symposium, Colorado Springs, CO, Sept. 29-Oct. 1, 1980, AGARD-CP-291.

2. Cline, M. C., "VNAP2: A Computer Program for Computation of Two-Dimensional, Time-Dependent, Compressible, Turbulent Flow," Los Alamos National Laboratory report LA-8872, Aug. 1981.

3. Cline, M. C., "VNAP: A Computer Program for Computation of Two-Dimensional, Time-Dependent, Compressible, Viscous, Internal Flows," Los Alamos National Laboratory report LA-7326, Nov. 1978.

4. Launder, B. E., Morse, A., Rodi, W., and Spalding, D. B., "The Prediction of Free Shear Flows - A Comparison of the Performance of Six Turbulence Models," NASA SP-321, Vol. I, pp. 361-426, 1973.

5. Cebeci, T., Smith, A. M. O., and Mosinskis, G., "Calculation of Compressible Adiabatic Turbulent Boundary Layers," AIAA J. 8, pp. 1974-1982, Nov. 1970.

6. Daly, B. J., unpublished notes, Los Alamos National Laboratory, 1972.

7. Jones, W. P. and Launder, B. E., "The Prediction of Laminarization With a Two-Equation Model of Turbulence," Int. J. Heat Mass Transfer 15, pp. 301-314, 1972.

8. Jones, W. P. and Launder, B. E., "The Calculation of Low-Reynolds-Number Phenomena with a Two-Equation Model of Turbulence," Int. J. Heat Mass Transfer 16, pp 1119-1130, 1973.

9. Launder, B. E. and Sharma, B. I., "Application of the Energy-Dissipation Model of Turbulence to the Calculation of Flow Near a Spinning Disc," Letters Heat Mass Transfer 1, pp. 131-137, 1974.

10. Hanjalic, K. and Launder, B. E., "Contribution Towards a Reynolds-Stress Closure for Low-Reynolds-Number Turbulence," J. Fluid Mech. 74, pp. 593-610, 1976.

11. Hung, C. M. and MacCormack, R. W., "Numerical Solutions of Supersonic and Hypersonic Laminar Compression Corner Flows," AIAA J. 14, pp. 475-481, April 1976.

12. MacCormack, R. W., "The Effect of Viscosity in Hypervelocity Impact Cratering," AIAA Paper 69-354, Cincinnati, Ohio, April 1969.

13. Harlow, F. H. and Amsden, A. A., "A Numerical Fluid Dynamics Calculation Method for All Flow Speeds," J. of Comp. Phys. 8, pp. 197-213, Oct. 1971.

14. MacCormack, R. W., "A Rapid Solver for Hyperbolic Systems of Equations," Lecture Notes in Physics 59, pp. 307-317, 1976.

15. Serra, R. A., "Determination of Internal Gas Flows by a Transient Numerical Technique," AIAA J. 10, 603-611, May 1972.

16. Oliger, J. and Sundström, A. "Theoretical and Practical Aspects of Some Initial Boundary Value Problems in Fluid Dynamics," SIAM J. of Applied Mathematics 35, pp. 419-445, Nov. 1978.

17. Moretti, G. and Abbett, M., "A Time-Dependent Computational Method for Blunt Body Flows," AIAA J. 4, pp. 2136-2141, Dec. 1966.

18. Rudy, D. H. and Strikwerda, J. C., "A Nonreflecting Outflow Boundary Condition for Subsonic Navier-Stokes Calculations," J. of Comp. Phys. 36, pp. 55-70, June 1980.

19. Mason, M. L., Putnam, L. E. and Re, R. J., "The Effect of Throat Contouring on Two-Dimensional, Converging-Diverging Nozzles at Static Conditions," NASA TP-1704, Aug. 1980.

20. Reubush, D. E., "Experimental Study of the Effectiveness of Cylindrical Plume Simulators for Predicting Jet-On Boattail Drag at Mach Numbers up to 1.30," NASA TN D-7795, 1974.

21. Swanson, R. C., "Numerical Solutions of the Navier-Stokes Equations for Transonic Afterbody Flows," NASA-TP-1784, Dec. 1980.

22. Mason, M. L. and Putnam, L. E., "Pitot Pressure Measurements in Flow Fields Behind Circular-Arc Nozzles With Exhaust Jets at Subsonic Free-Stream Mach Numbers," NASA TM-80169, Dec. 1979.

23. Wilmoth, R. G., "Viscous-Inviscid Calculations of Jet Entrainment Effects on the Subsonic Flow Over Nozzle Afterbodies," NASA-TP-1626, April 1980.

24. Re, R. J., "An Investigation of Several NACA 1-Series Inlets at Mach Numbers From 0.4 to 1.29 for Mass-Flow Ratios Near 1.0," NASA TM X-3324, Dec. 1975.

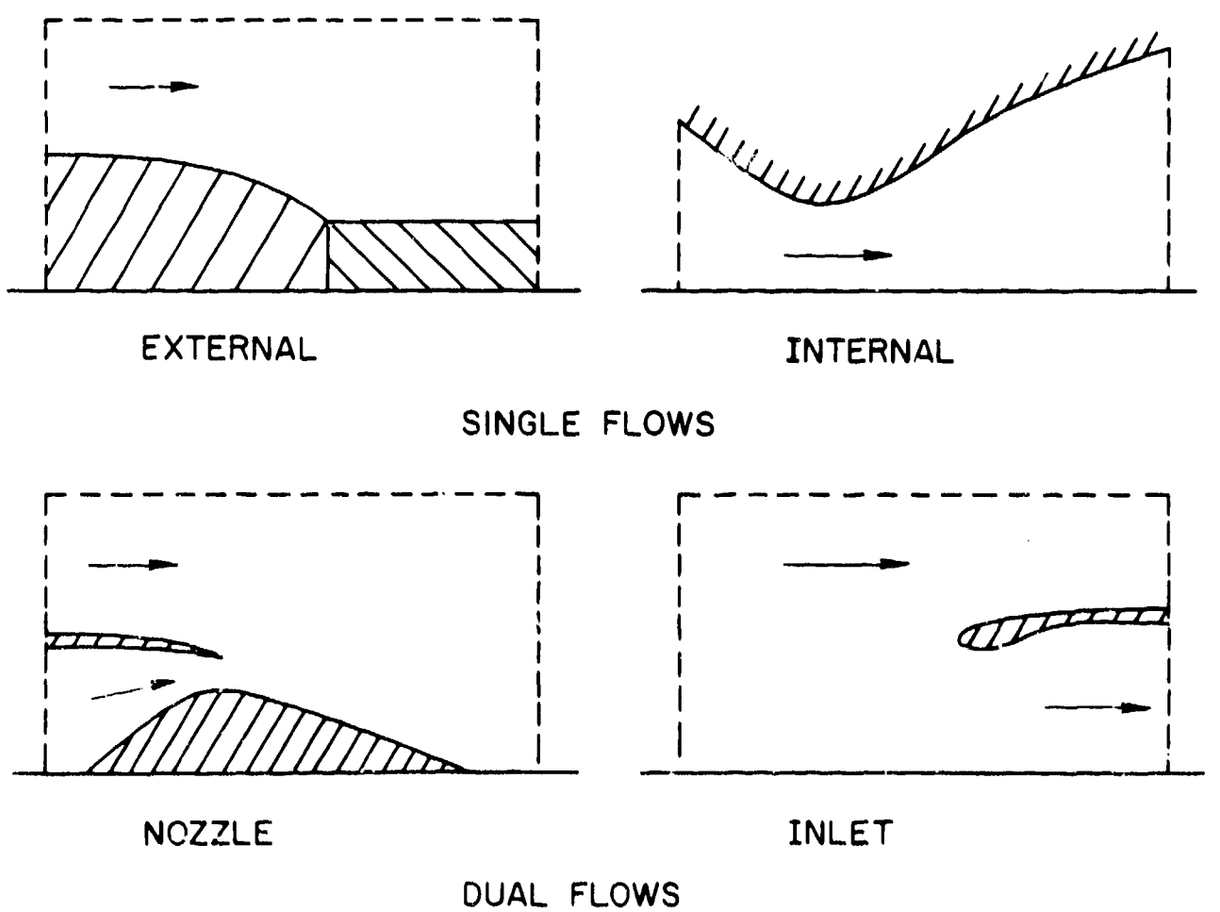

Fig. 1. Typical internal, external and internal/external geometries.

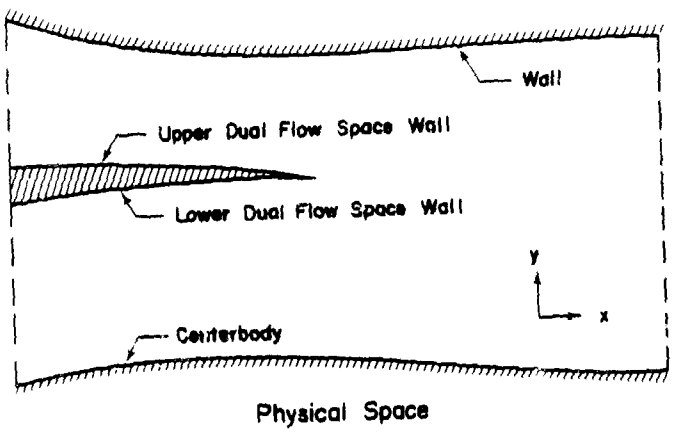

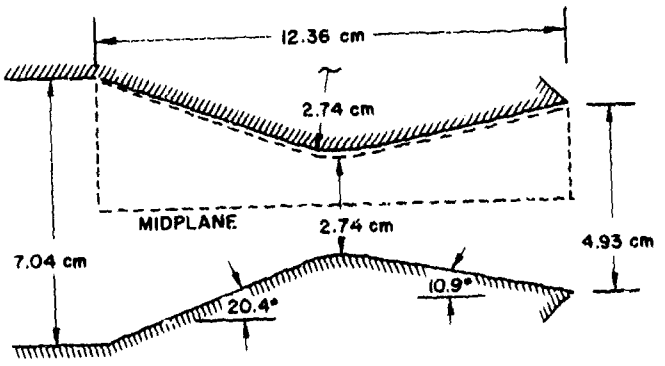

Fig. 4. Internal flow geometry.

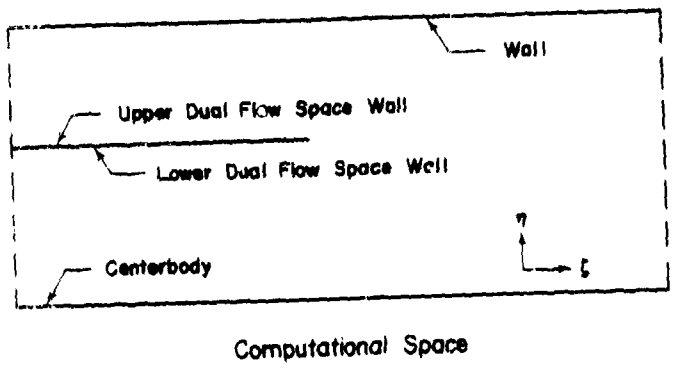

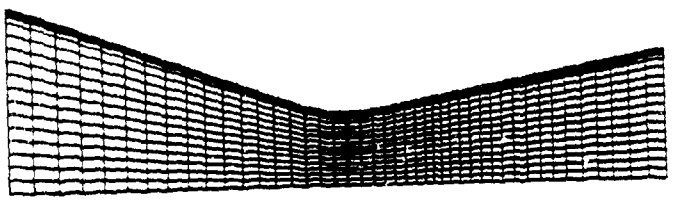

Fig. 2. Physical and computational spaces.

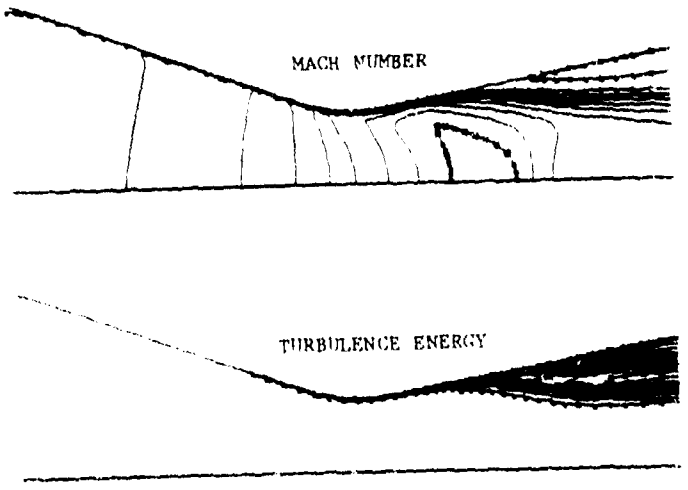

Fig. 5. Internal flow physical space grid, Mach number and turbulence energy contours.

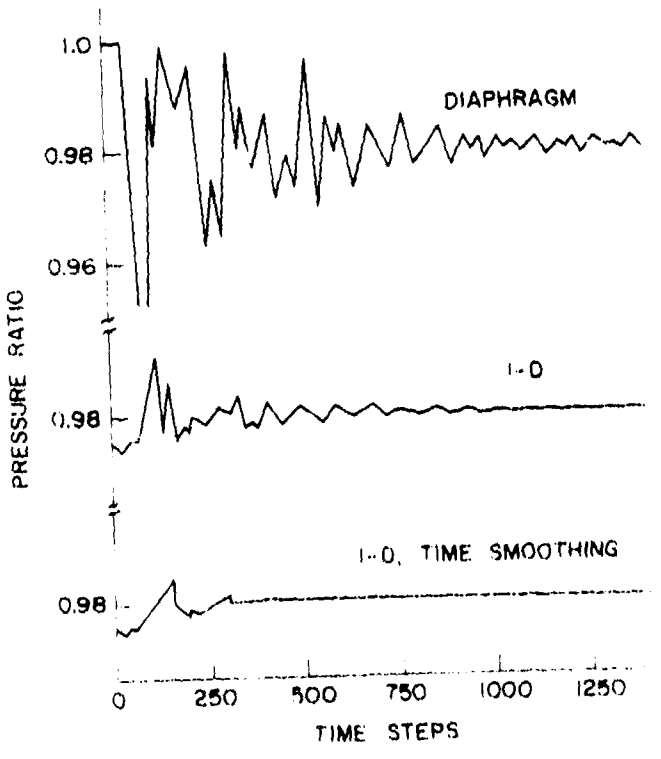

Fig. 3. Pressure ratio vs time step for subsonic flow in a converging duct.

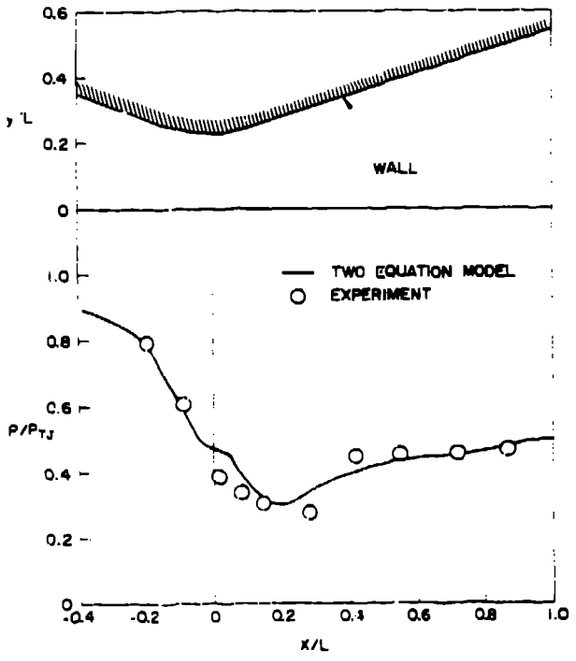

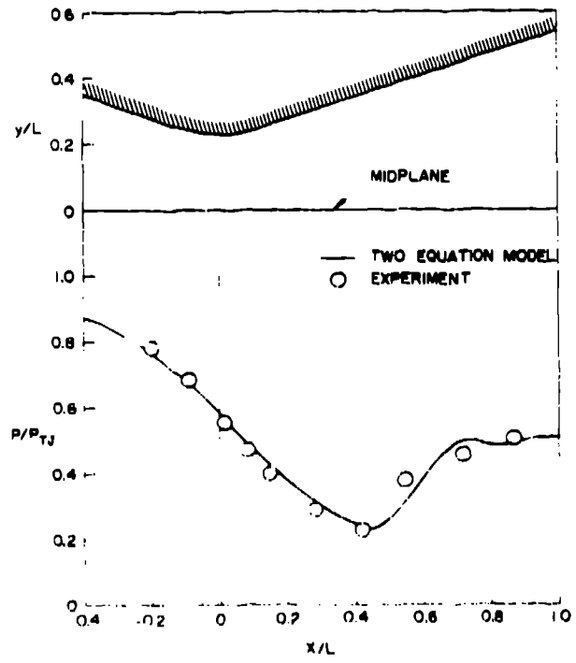

Fig. 6. Internal flow wall (top) and midplane pressure ratio (L=5.98 cm).

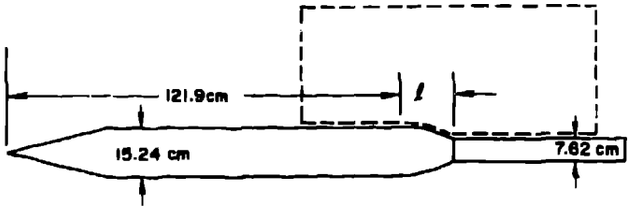

Fig. 7. External flow geometry.

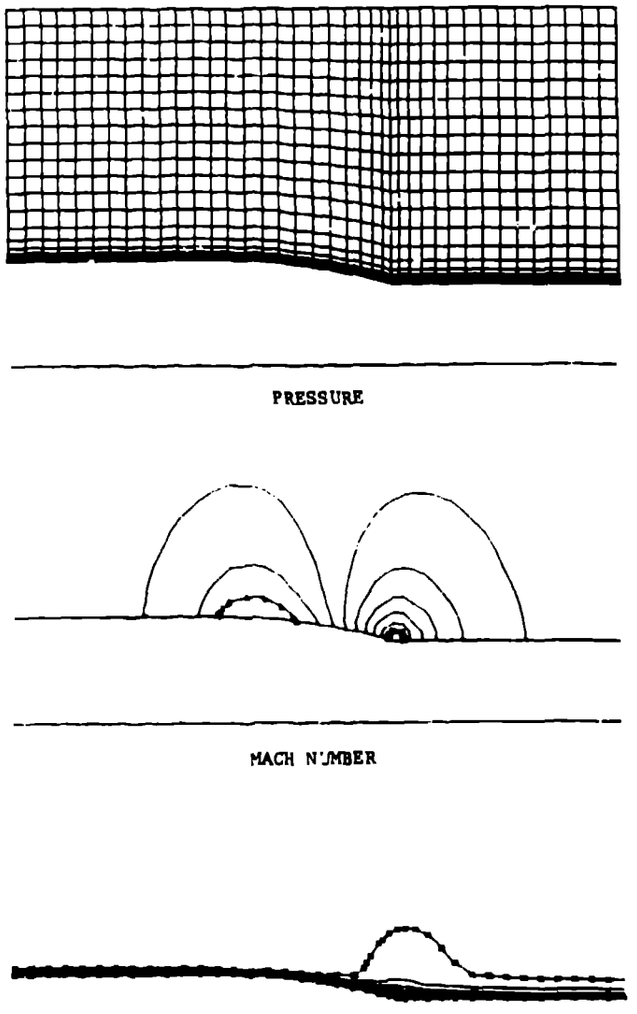

Fig. 8. External flow (config. 3) physical space grid, pressure and Mach number contours.

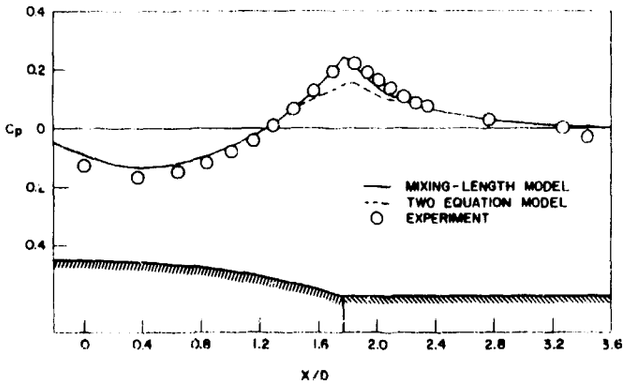

Fig. 9. External flow (config. 3) surface pressure coefficient (D=15.24 cm).

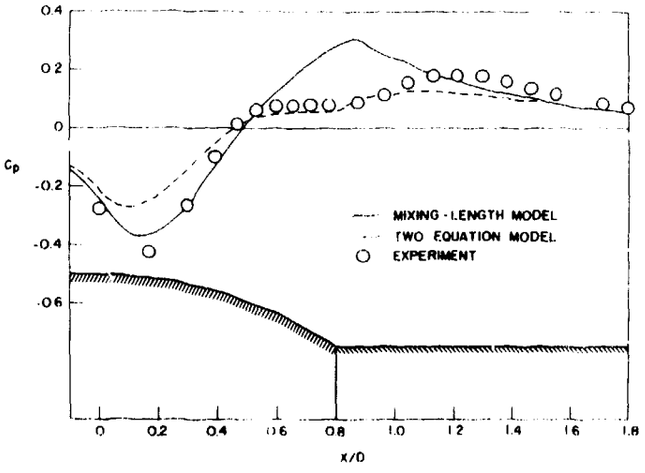

Fig. 11. External flow (config. 1) surface pressure coefficient (D=15.24 cm).

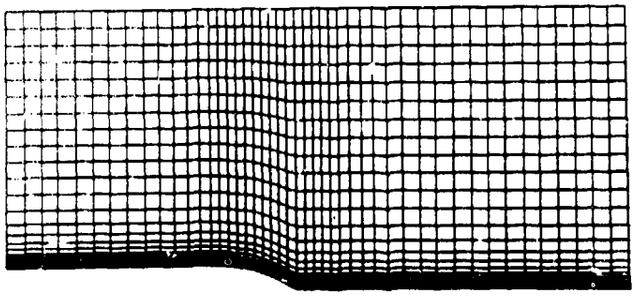

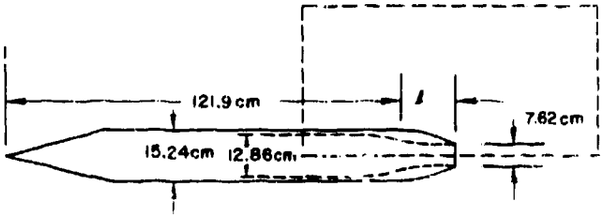

Fig. 12. Internal/external flow afterbody geometry.

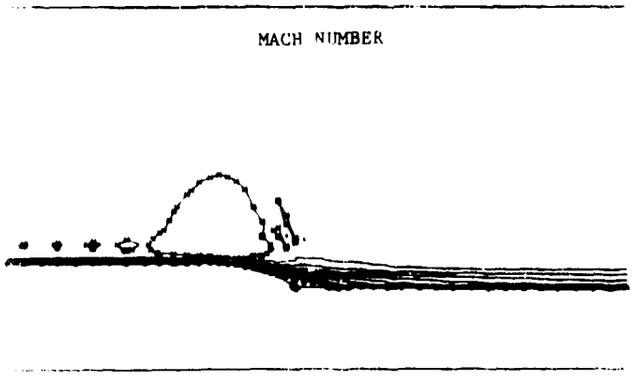

Fig. 10. External flow (config. 1) physical space grid, Mach number and turbulence energy contours.

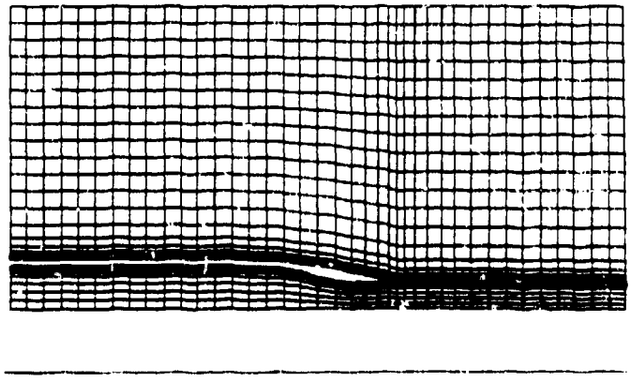

Fig. 13. Internal/external flow (config. 3) physical space grid and Mach number.

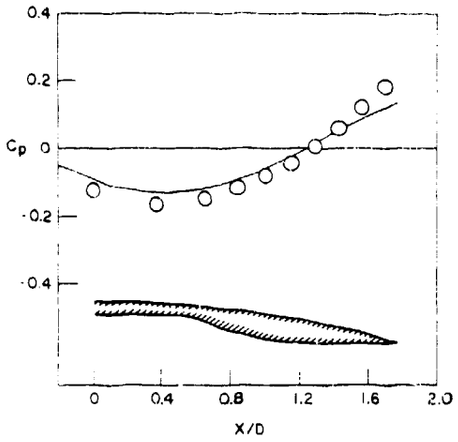

Fig. 14. Internal/external flow (config. 3) external surface pressure coefficient (D=15.24 cm).

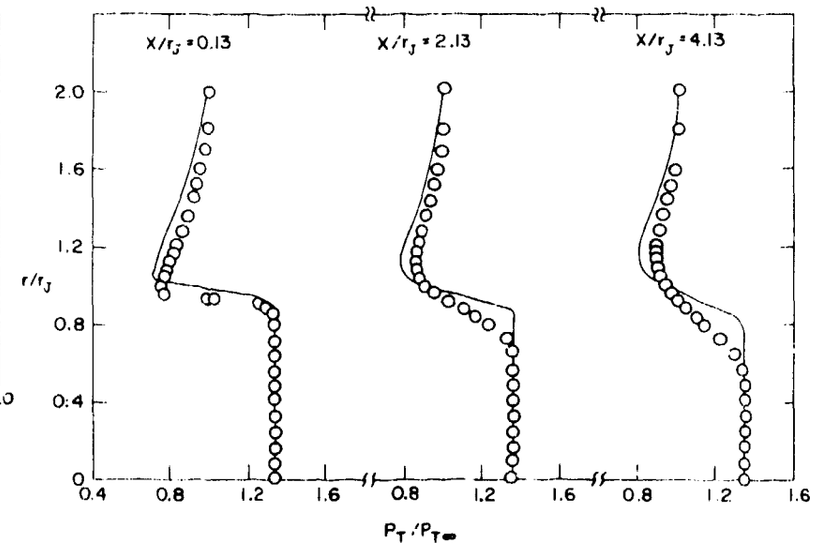

Fig. 15. Internal/external flow (config. 3) total pressure ratio profiles in the shear layer (x is measured from the exit and r_J=3.81 cm).

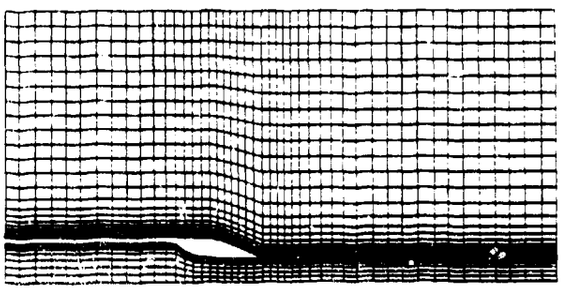

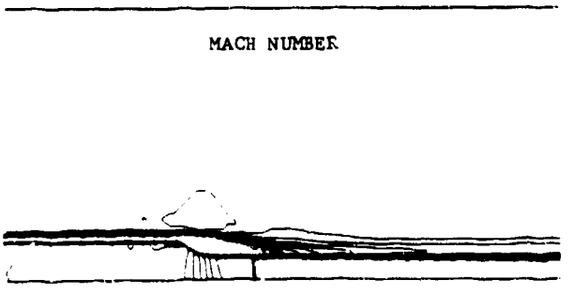

Fig. 16. Internal/external flow (config. 1) physical space grid and Mach number.

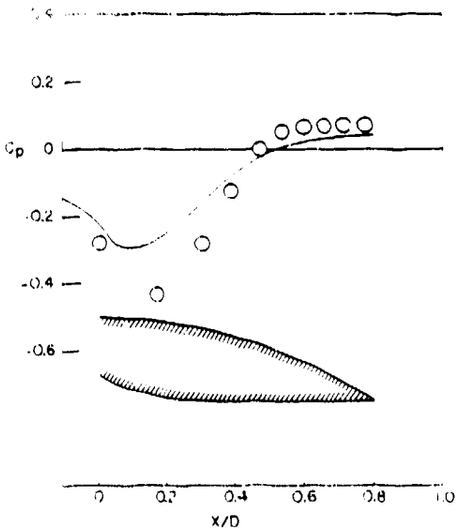

Fig. 17. Internal/external flow (config. 1) external surface pressure coefficient (D=15.24 cm).

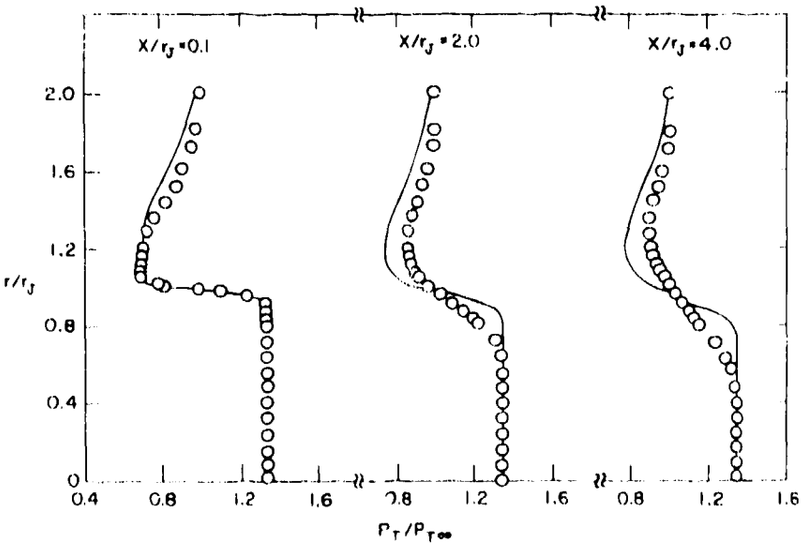

Fig. 18. Internal/external flow (config. 1) total pressure ratio profiles in the shear layer (x is measured from the exit and r_J=3.81 cm).

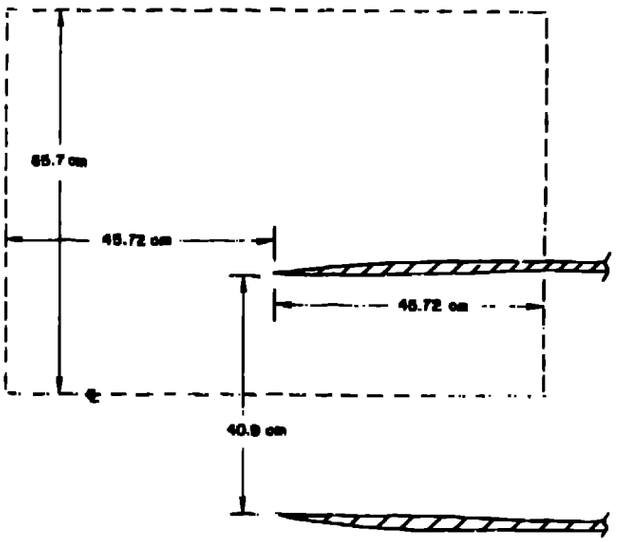

Fig. 19. Internal/external flow inlet geometry.

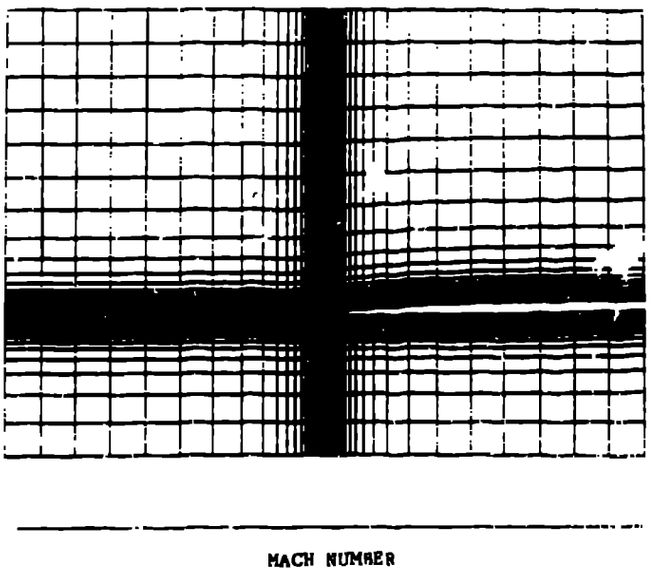

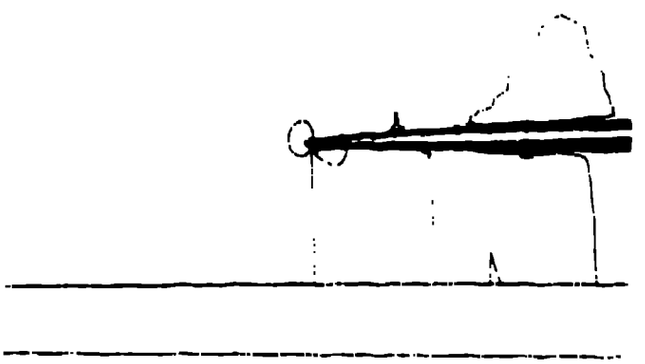

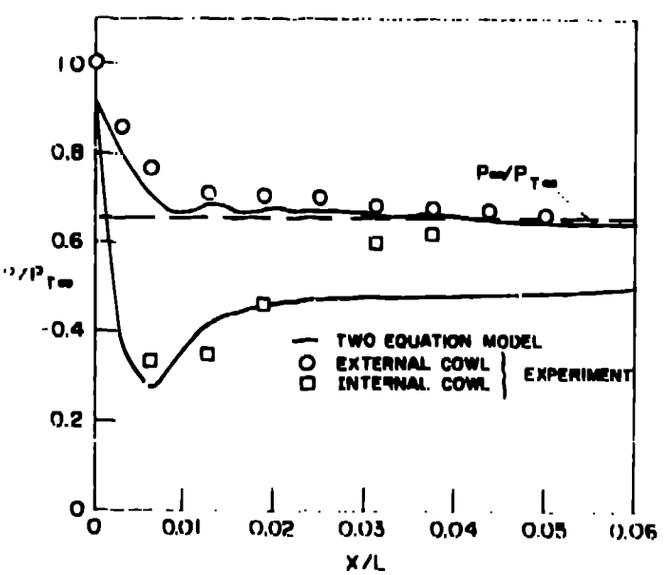

Fig. 21. Internal/external flow (inlet) surface pressure (L=45.72 cm).

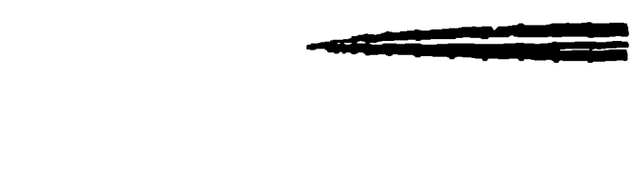

Fig. 20. Internal/external flow (inlet) physical space grid, Mach number and turbulence energy.